Journal of Bio- and Tribo-Corrosion (2021) 7:80
https://doi.org/10.1007/s40735-021-00519-2

Erosion-Corrosion Mechanisms of Engineering Steels in Different NaCl Concentrations

F. Brownlie[1,2] · T. Hodgkiess[3] · A. Pearson[4] · A. M. Galloway[1]

Received: 20 January 2021 / Revised: 29 March 2021 / Accepted: 5 April 2021 / Published online: 20 April 2021

Abstract

This study utilises a recently developed, enhanced approach to assess detailed aspects of the corrosive wear behaviour of different steel grades in aqueous slurries containing three NaCl concentrations (0.05%NaCl, 3.5%NaCl and 10%NaCl). Erosion-corrosion testing was conducted using a slurry impingement test rig and damage was quantified using volume loss, potentiodynamic polarisation scans and surface topography. Single- and segmented specimens were adopted to yield the contribution of the degradation mechanisms in the two hydrodynamic zones (directly impinged and surrounding area). The overall material losses from the two zones of the stainless steels were observed to increase with increasing salinity. However, the overall material loss for the low-alloy steel was found to increase from 0.05%NaCl to 3.5%NaCl, before reducing when the salinity was further increased to 10%NaCl. Changes in salinity were observed to have the most effect on the corrosion-enhanced mechanical damage mechanism. The in-house developed technique demonstrated good linkage between single samples and the outer area damage region. However, it also showed that the use of single samples can be less successful when assessing highly turbulent (directly impinged) damage regions.

Keywords Erosion-corrosion · Steel · Stainless steel · Salinity

1 Introduction

Corrosive wear is a substantial issue for many industrial components operating in the oil/gas and mineral ore extraction sectors. Such components (for instance, fluid handling equipment such as pumps, valves, pipes, etc.) have to operate in a wide range of conditions and are commonly in contact with aqueous solutions. The solutions can have a varied chemical composition dependent upon the industrial process as well as geographical location [1]. Therefore, the total dissolved salts (TDS)—often referred to as "salinity"—in the aqueous solution can range from extremely low levels (less than 50 mg/l) in freshwater to highly saline brines (5% TDS and above). Also, the increasing demand and scarcity of freshwater is requiring industry to utilise and recycle high saline solutions [2–4].

The use of higher TDS solutions in industry will have an impact on the durability of components. Therefore, it is clear that the effect of salinity on common engineering materials needs to be studied. As it is also common for such industrial components to be transporting solid particles along with the aqueous solution, then it is also prevalent to understand how salinity will affect the corrosive wear process.

Previous corrosive wear studies have focussed on a single-salinity aqueous solution, typically 3.5%NaCl [5, 6]. Some previous work has evaluated two different salinities (0.05%NaCl and 3.5%NaCl) [7–10] but there appears to be an absence of literature on the effects of salt concentration above 3.5%NaCl.

With regard to the effect of salt concentration on the pure corrosion behaviour of iron, carbon- and low-alloy steels, there is a general consensus that, in low-turbulent, solids-free, neutral and low pH conditions [11–15], there is an increase in corrosion rate with increased NaCl content, before the corrosion rates decrease above a certain salt concentration. The reported value of the salt concentration associated with this maximum corrosion rate varies between

✉ F. Brownlie
frazer.brownlie@mail.weir

1 Department of Mechanical & Aerospace Engineering, University of Strathclyde, Glasgow, UK

2 Weir Advanced Research Centre, Glasgow, UK

3 School of Engineering, University of Glasgow, Glasgow, UK

4 Ascott Metallurgical Ltd, Glasgow, UK

the different studies. In low pH conditions, the maximum rate is reported to occur at 1%NaCl or less [14, 15]; however, in neutral conditions, the peak is reported to occur between 1% and 3%NaCl [11–13]. Although some of these differences can be attributed to factors such as variations in the cathodic reactions over a range of pH, some debate remains on the correlations between salt concentration and consequent corrosion rate [14, 16]. It is clear that there is a lack of information and understanding on the effect of salinity on pure corrosion – and even more so on corrosive wear—of commonly used engineering materials.

An important aspect of this assessment, of the response of materials to various levels of salinity in the fluid, is that it is dependent upon a number of factors:-

- The complexity of the corrosive wear process- being dependent upon a number of deterioration mechanisms that contribute to the overall damage, T summarised as follows [17–20]:

$$T = M + C + \Delta M_c + \Delta C_m \quad (1)$$

where M is the pure mechanical damage, C is the pure corrosion component and the two terms, ΔMc (corrosion-enhanced mechanical damage) and ΔCm (mechanically enhanced corrosion), often called "synergy", signify the interactive factors involved in corrosive wear which often represent a substantial contribution to overall damage,

- The nature of the hydrodynamic conditions, which can vary from highly turbulent in the region directly impinged by a fluid (DIZ) and the surrounding areas (OA) in which the conditions are much less severe [21].
- Taking the hydrodynamic feature into account, the total material loss now becomes [21]:-

$$TVL = E_{DIZ} + C_{DIZ} + \Delta C_{m\,DIZ} + \Delta M_{c\,DIZ} + SA_{OA} + C_{OA} + \Delta C_{m\,OA} + \Delta M_{c\,OA} \quad (2)$$

where TVL is the total volume loss, E_{DIZ} represents the pure mechanical erosion damage, C_{Diz} is the pure corrosion damage, $\Delta C_{m\,DIZ}$ is the corrosion-enhanced-by-mechanical damage and $\Delta M_{c\,DIZ}$ is the mechanical-enhanced-by-corrosion damage, all occurring within the DIZ. The damage mechanisms in the outer area are given by - SA_{OA} signifying the low-angle sliding abrasion damage, C_{OA} is the pure corrosion damage, $\Delta C_{m\,OA}$ is the corrosion-enhanced-by-mechanical damage and $\Delta M_{c\,OA}$ is the mechanical-enhanced-by-corrosion damage

- The relative extents of the various damage terms in Eq. (2) are likely to vary on materials upon the surface of which a passive film does or does not form.

In a previous paper [22], the focus was on the role of salinity on the overall material losses – as expressed by Eq. (1). The effect of salinity on corrosion behaviour of passive- and non-passive materials was subject to a subsequent detailed study [16]. The purpose of the present paper is to identify how the various components that contribute (via Eq. 2) to erosion-corrosion damage are themselves subject to the influences of different salinities in the two distinct hydrodynamic zones associated with an impinging, solids-laden stream. To properly identify the interrelating effects of salinity and hydrodynamic conditions, this assessment has comprised the study of two types of specimen.

- Measurements on the single specimens (38 mm dia.)
- Analysing the behaviour of segmented specimens which facilitates comparisons of features in the directly impinged zone (DIZ) and outer regions of the specimen—thereby taking into account the different hydrodynamic zones which occur during the impingement test—and which reflect most operational circumstances

Thus, using this enhanced analytical technique [21] it is possible to obtain a deeper understanding of the different degradation processes occurring and how the salinity is influencing these mechanisms. Recognition of the role of the different factors on erosion-corrosion in liquids of varying salinities should represent a useful contribution to assessments of the durability of engineering alloys in such a range of water compositions. This study contains four commonly used engineering materials; a high-strength, low-alloy steel (UNS G43400), and three grades of stainless steel (Materials & methods section). The erosion-corrosion tests were conducted in a submerged, recirculating, impingement slurry-jet test rig.

2 Materials and Methods

The four alloys considered in this study comprised a high-strength low-alloy steel (UNS G43400), a precipitation hardened martensitic stainless steel (UNS S15500), an austenitic stainless steel (UNS S31600) and a superduplex stainless steel (UNS S32760). The nominal chemical composition of each steel is presented in Table 1, and the measured hardness, nominal density, heat treatment condition and microstructural constituents of each steel are

displayed in Table 2. The test materials were supplied by commercial vendors in rod form.

Solid–liquid impingement tests were conducted in free erosion-corrosion (FEC) conditions using a recirculating, submerged, impingement slurry-jet test rig [23]. The duration of the tests was 1 h. Slurry was impinged upon the central regions of specimens (38 mm dia.) at an angle of 90° through a nozzle of 4 mm diameter at 18 m/s with a temperature of 40 ± 1 °C. The nozzle was offset from the specimen surface by 5 mm. Three slurries were employed to observe the effect of salinity and they consisted of 500 µm spherical silica sand particles suspended in 0.05%NaCl, 3.5%NaCl or 10%NaCl aqueous solution. The sand concentration was measured to be 0.5 g/l. The sand size distribution and example of sand particle geometry is given in Fig. 1. The specimens were ground to 1200 grit paper prior to testing. The mass loss of the test samples was measured using a calibrated Sartorius Entris mass balance with an accuracy of ± 0.1 mg. A minimum of two test replicates was conducted for each test material and condition.

In situ potentiodynamic polarisation scans [16] were carried out to assess the electrochemical corrosion rates of the materials in all test conditions. Potentiodynamic polarisation

Table 1 Nominal chemical compositions (%wt) of the tested materials

Material	C	Cr	Ni	Mn	Si	Mo	S	N	P	Cu	W	Nb	Fe
UNS G43400	0.37–0.43	0.7–0.9	1.65–2	0.6–0.8	0.15–0.3	0.2–0.3	0.04	–	0.035	–	–	–	Bal
UNS S15500	0.07 max	14–15.5	3.5–5.5	1 max	1 max	-	0.03 max	–	0.04	2.5–4.5	–	0.15–0.45	Bal
UNS S31600	0.08 max	16–18	10–14	2 max	0.75 max	2–3	0.03 max	0.1 max	0.045 max	–	–	–	Bal
UNS S32760	0.03 max	24–26	6–8	1 max	1 max	3–4	0.01 max	0.2–0.3	0.03 max	0.5–1	0.5–1	–	Bal

Table 2 Measured hardness, nominal densities, heat treatment condition and microstructural constituents of the tested materials

Material	Hardness (HV–5kgf)	Density (g/cm^3)	Heat treatment condition	Microstructural constituents
UNS G43400	300	7.85	Quenched & tempered	Martensitic
UNS S15500	360	7.80	Solution annealed & age hardened	Martensitic with retained austenite
UNS S31600	170	8.00	Annealed	Austenitic with delta ferrite stringers
UNS S32760	265	7.80	Annealed	Ferrite/austenite duplex structure

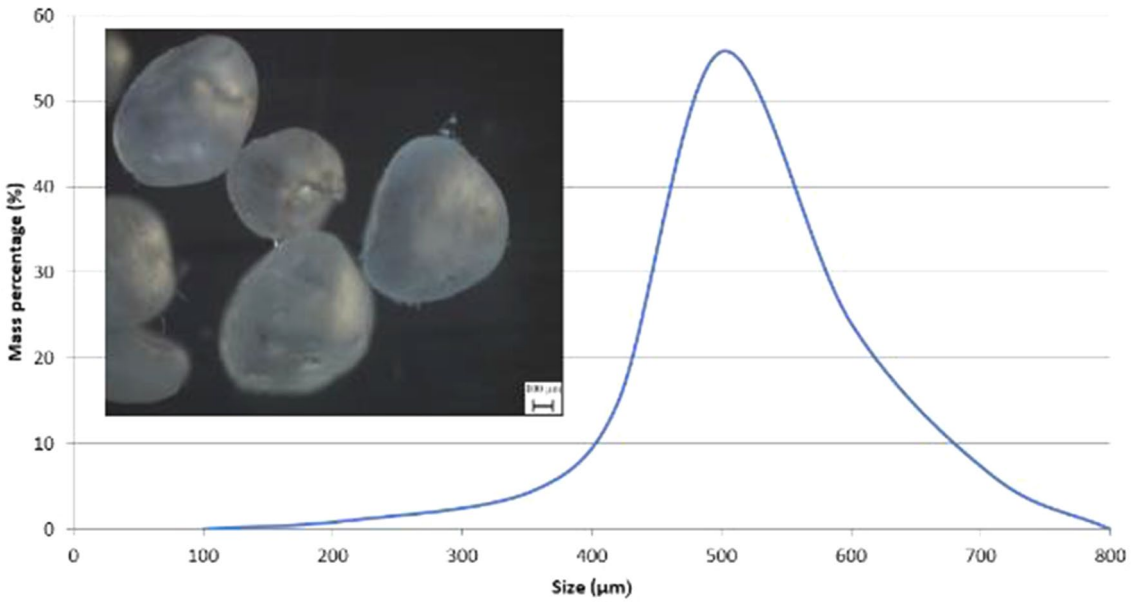

Fig. 1 Sand size distribution and example of shape of sand particles

scans were also conducted in static conditions in order to evaluate the erosion-enhanced corrosion mechanisms. The corrosion monitoring exercises, undertaken in static solution, were also undertaken in the jet impingement rig but in quiescent conditions.

The polarisation tests were conducted 15 min after the sample was submerged to allow for the free electrode potential, E_{corr}, to stabilise. A Gill AC potentiostat was utilised for the potentiodynamic scans. Platinum was used for the auxiliary electrode and Ag/AgCl was employed as the reference electrode. The tests were conducted by shifting the initial electrode potential either 20 mV more positive (cathodic) or 20 mV more negative (anodic) than the free electrode potential, hence ensuring that the transition point (the free corrosion potential, E_{corr}) would be captured. Scans then continued to 300 mV more negative (cathodic) or 300 mV more positive (anodic) at a sweep rate of 10 mV/min. The chosen ranges were sufficient to evaluate corrosion current measurements by way of Tafel extrapolation. The measured current densities were then used to evaluate the associated mass losses due to corrosion via calculation using Faraday's Law and the so-calculated mass losses were converted to a volume loss using the nominal density of the respective steels.

To conduct the polarisation tests, an electrically conductive wire was connected to the rear of the specimens, which were then cold mounted in epoxy resin. This ensured that only the directly exposed surface was corroding. Segmented samples were also used to determine the disparate corrosion rates in the directly impinged zone (DIZ) and outer area (OA) of the specimens. The segmented samples were created by cutting a 5 mm diameter cylinder from the centre of the specimen onto which the jet would impinge (DIZ). The sides of this cylinder were insulated with a polymer to prevent electrical connection between the DIZ and OA, and both regions were separately connected to an electrically conductive wire as with the full polarisation samples. The layout and dimensions of these segmented samples is shown in Fig. 2. An example of a potentiodynamic polarisation scan for a segmented UNS S15500 sample (with Tafel extrapolation lines) is shown in Fig. 3 and illustrates the substantial difference in corrosion behaviour in the two hydrodynamic zones. Figure 4 displays an example of potentiodynamic polarisation scan replicates for UNS S31600 in 3.5%NaCl static conditions. The experimental error in the i_{corr} value was observed to be approximately 5%.

Impressed current cathodic protection (ICCP) tests were also performed to isolate the pure mechanical damage by maintaining the electrode potential at -800 mV using an Ag/AgCl reference electrode. Back extrapolation of the anodic polarisation curves at this potential demonstrated that the residual anodic reaction rates were negligible, as has been observed in a previous study [22].

The wear scar topography of the tested materials (FEC and ICCP) was assessed using an Alicona InfiniteFocus 3D optical profilometer with a wear scar volume accuracy of $\pm 0.02 mm^3$. This procedure facilitated the separation of the material losses between the DIZ and OA regions (as described in Eq. 2).

A feature of submerged jet experiments, conducted on single specimens, in which the area of the directly impinged zone is less than the overall area, is that the findings essentially represent an "average" of effects experienced in distinctly different hydrodynamic regions and therefore mask any behavioural differences between these two distinct regions. The potential benefit of the procedures described above—involving electrochemical monitoring of segmented specimens and the surface profiling measurements—is to provide a means of differentiating trends in material loss extents and mechanisms associated within the two zones [21, 23].

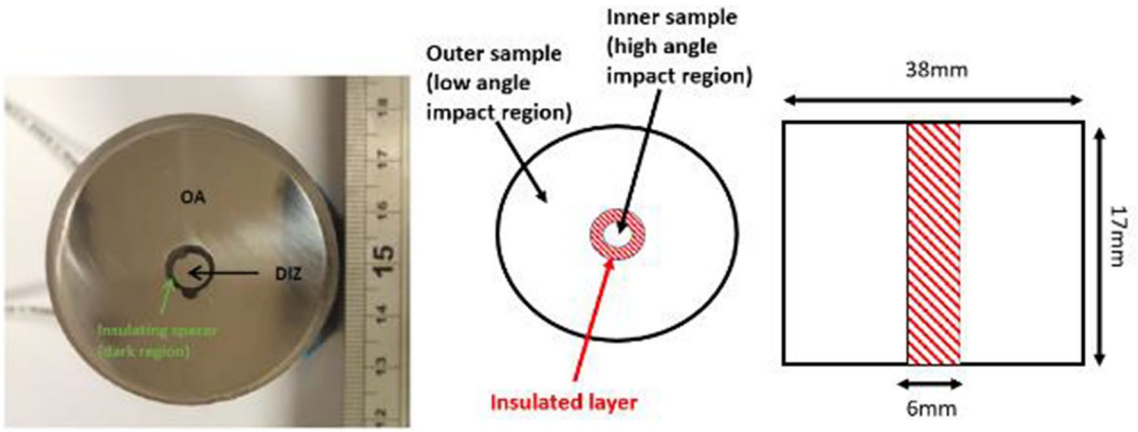

Fig. 2 Segmented sample encapsulated in epoxy resin

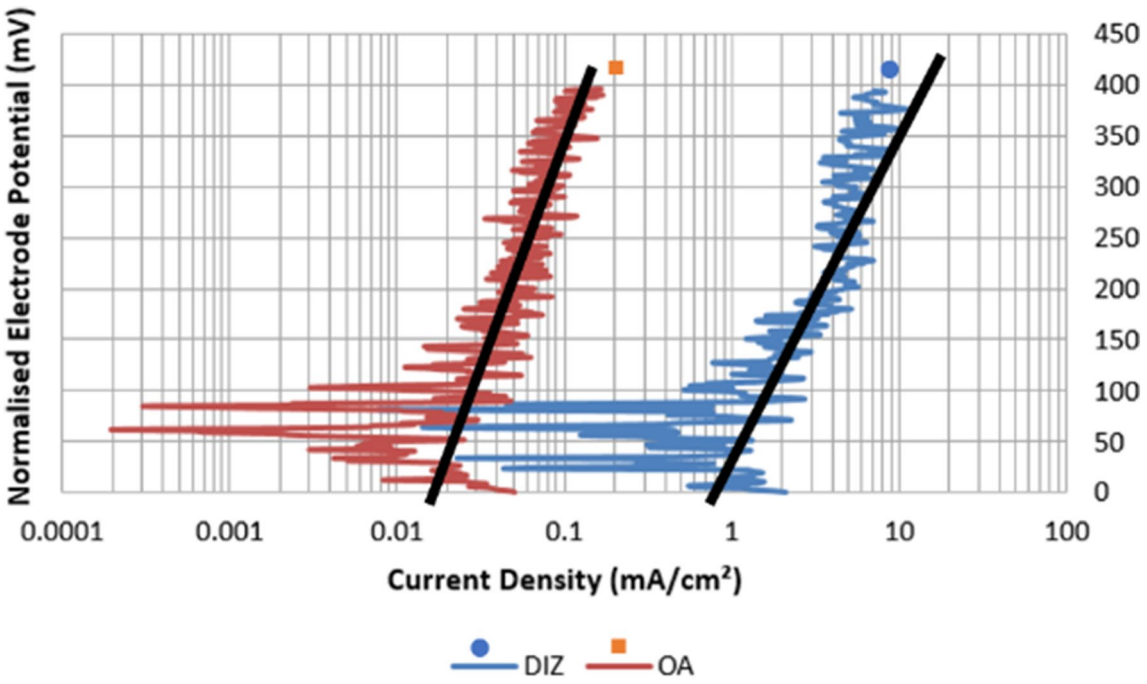

Fig. 3 Example of potentiodynamic polarisation scan for segmented UNS S15500 in 3.5%NaCl solid–liquid impingement conditions

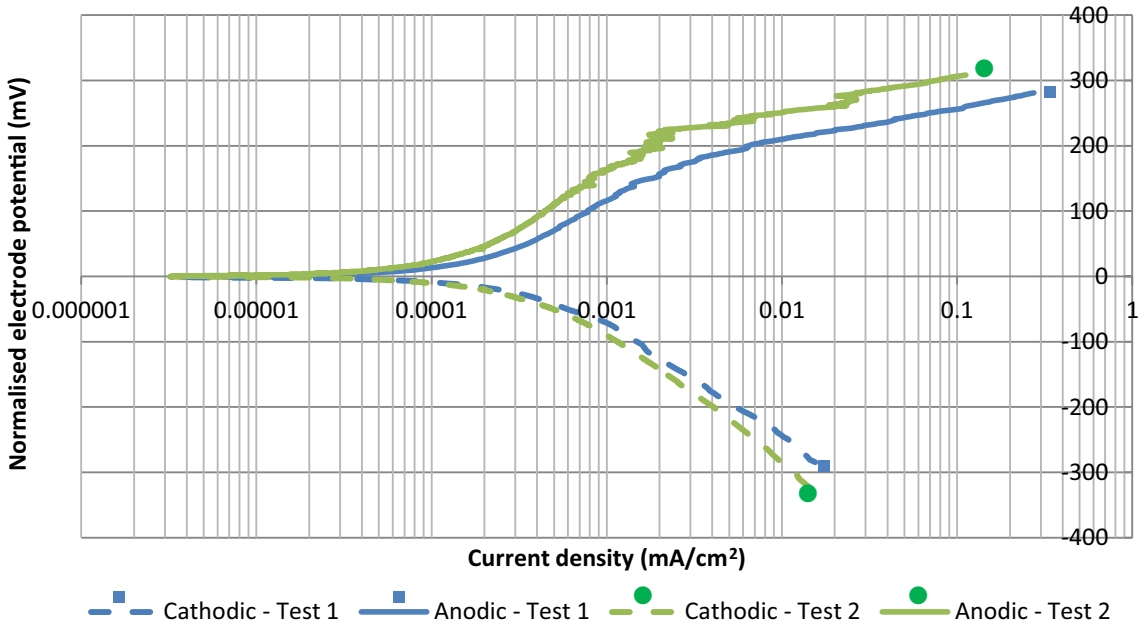

Fig. 4 Example of potentiodynamic polarisation scan repetitions for UNS S31600 in 3.5%NaCl static conditions

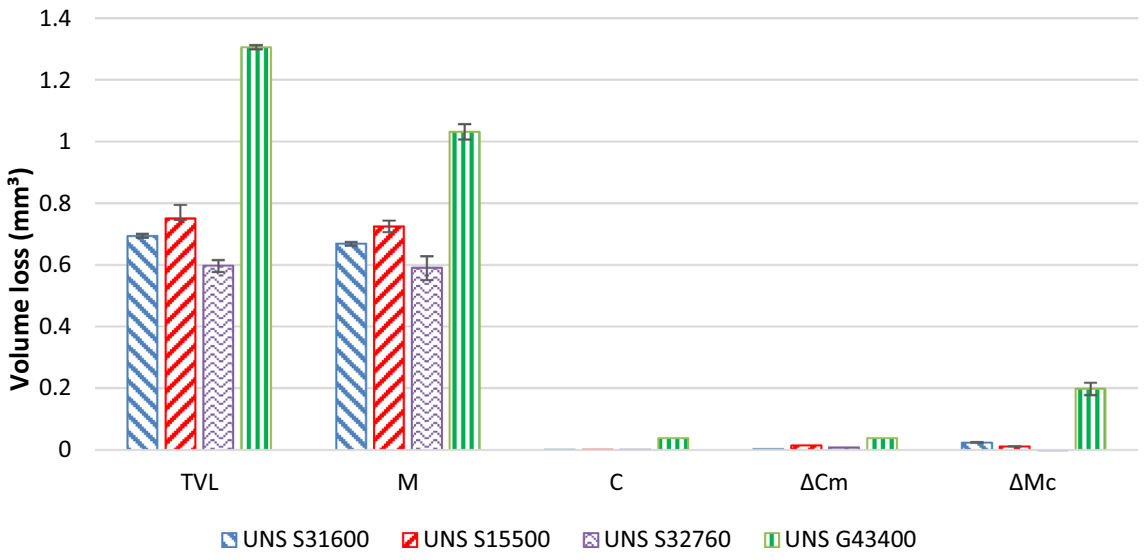

Fig. 5 Mechanism breakdown for full samples in 0.05%NaCl

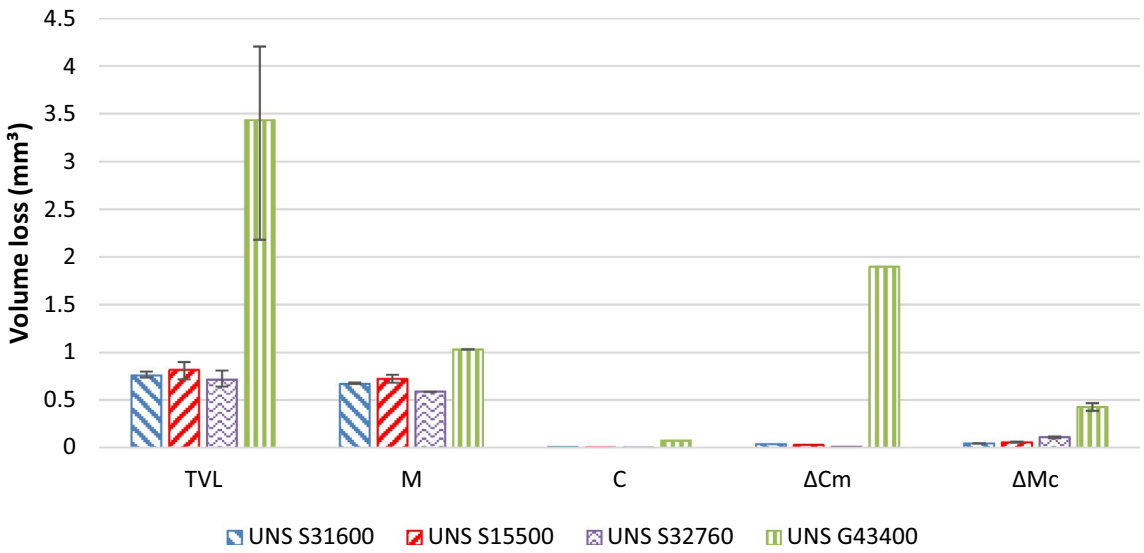

Fig. 6 Mechanism breakdown for full samples in 3.5%NaCl

3 Results and Discussion

3.1 Mechanistic Breakdown of M, C, ΔMc and ΔCm for Full Size Samples

Figures 5, 6, 7 display the findings from measurements and calculations on single specimens of all four alloys. TVL and M are measured under FEC and CP conditions respectively, ΔC_M is calculated from the difference in corrosion volume loss measured in FEC and static conditions, leaving the ΔM_C term as the only unknown in Eq. 1. For the low-alloy steel in 0.05%NaCl solution, the damage was predominantly mechanical in nature with very little pure corrosion, a small erosion-enhanced corrosion but a significant corrosion-enhanced erosion contribution. As the concentration of salt rises to 3.5%NaCl, there is a substantial increase in total material loss (TVL) which is accompanied by an increasing proportion of corrosion-related damage which accounts for approximately 60% of the total material loss in the more-saline conditions. An interesting feature is that the amount of pure corrosion is very small and the main contributors are the synergy terms in which erosion-enhanced corrosion (ΔC_m) is significant. A further increase in salt concentration

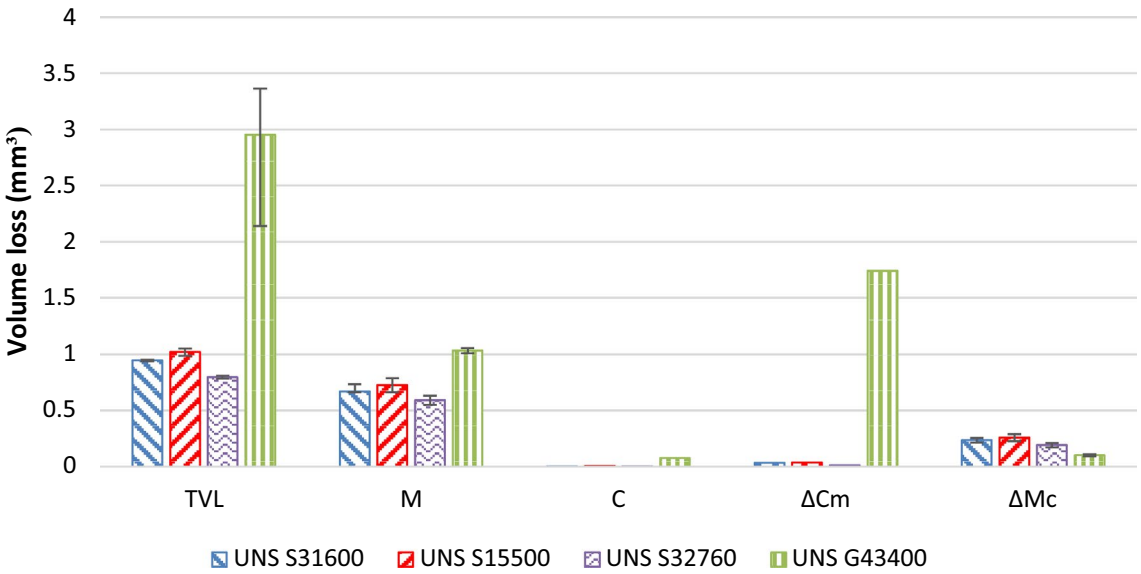

Fig. 7 Mechanism breakdown for full samples in 10%NaCl

to 10%NaCl leads to a decrease in total material loss which is associated with corresponding reductions in the magnitudes of the corrosion-related factors.

For the stainless steels, pure mechanical damage was predominant at all salt concentrations but with contributions from corrosion-enhanced erosion attributing to about 20% of damage in the most saline solution–despite a negligible role of pure corrosion.

Summarising the effect of salt concentration, perhaps unsurprisingly, there was no recorded influence on pure mechanical damage for either low-alloy or stainless steel. Increases in NaCl concentration did, however, bring about raised contributions of corrosion-related damage in all of the alloys. The volume loss caused by pure corrosion for the low-alloy steel, increased from 0.05%NaCl to 3.5%NaCl but with no further increase up to 10%NaCl. But, as a proportion of total metal loss, the pure corrosion contribution was extremely low (3%). Most of the corrosion-related damage was attributed to the two synergy terms with a dramatically increased contribution from mechanical-enhanced corrosion in the 3.5%NaCl solution—which did not, however, increase any further to 10%NaCl. Similar trends have been reported and discussed previously [16].

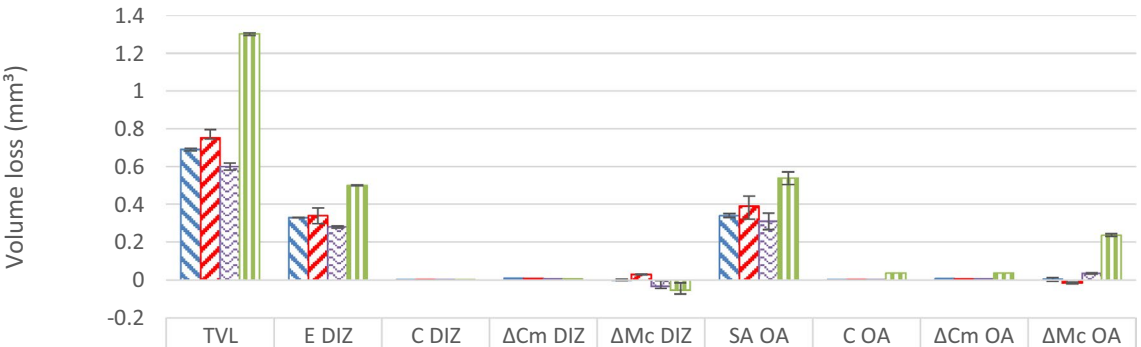

	TVL	E DIZ	C DIZ	ΔCm DIZ	ΔMc DIZ	SA OA	C OA	ΔCm OA	ΔMc OA
UNS S31600	0.69	0.33	0.000013	0.010	-0.0005	0.34	0.000721	0.01	0.004
UNS S15500	0.75	0.34	0.000011	0.006	0.0300	0.39	0.00058	0.01	-0.016
UNS S32760	0.60	0.28	0.000008	0.004	-0.0340	0.31	0.00044	0.005	0.035
UNS G43400	1.30	0.5	0.000668	0.005	-0.0553	0.54	0.03676	0.04	0.237

Fig. 8 Breakdown of corrosive wear for segmented sample in 0.05%NaCl

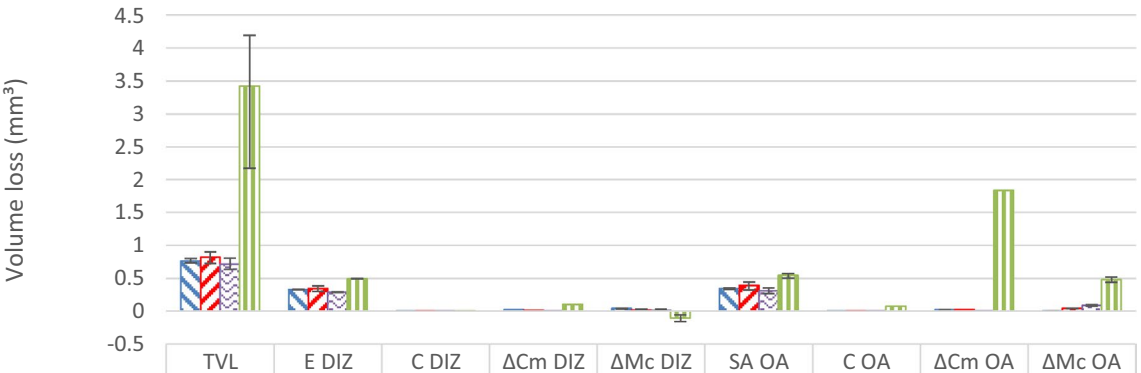

	TVL	E DIZ	C DIZ	ΔCm DIZ	ΔMc DIZ	SA OA	C OA	ΔCm OA	ΔMc OA
UNS S31600	0.76	0.33	0.00001	0.021	0.039	0.34	0.00072	0.021	0.01
UNS S15500	0.82	0.34	0.00005	0.013	0.017	0.39	0.00291	0.019	0.04
UNS S32760	0.71	0.29	0.00003	0.007	0.013	0.31	0.00178	0.004	0.08
UNS G43400	3.42	0.49	0.00134	0.106	-0.107	0.54	0.07351	1.837	0.48

Fig. 9 Breakdown of corrosive wear for segmented sample in 3.5%NaCl

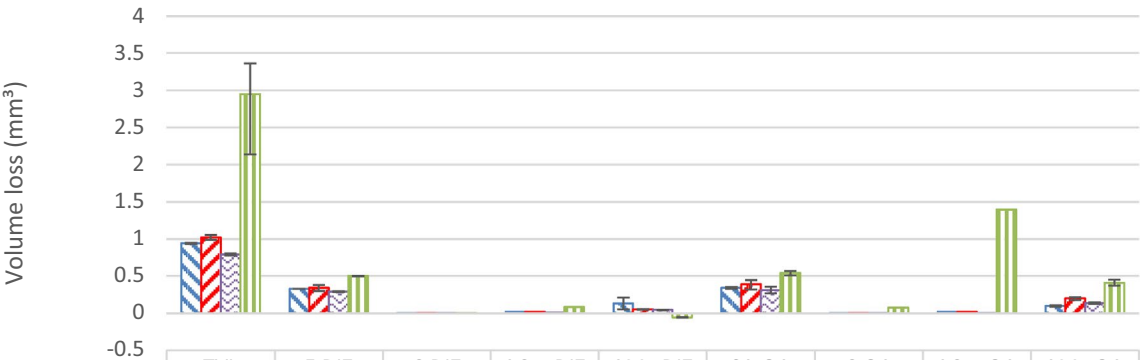

	TVL	E DIZ	C DIZ	ΔCm DIZ	ΔMc DIZ	SA OA	C OA	ΔCm OA	ΔMc OA
UNS S31600	0.94	0.33	0.00004	0.02	0.13	0.34	0.00216	0.019	0.10
UNS S15500	1.02	0.34	0.00011	0.02	0.05	0.39	0.00582	0.016	0.20
UNS S32760	0.79	0.29	0.00006	0.01	0.04	0.31	0.00326	0.003	0.13
UNS G43400	2.95	0.5	0.00134	0.08	-0.06	0.54	0.07351	1.396	0.41

Fig. 10 Breakdown of corrosive wear for segmented sample in 10%NaCl

3.2 Mechanistic Breakdown of M, C, ΔM_c and ΔC_m in Different Hydrodynamic Regions

Figures 8, 9, 10, detail the findings from the segmented samples which break down the degradation mechanisms further into the two different hydrodynamic regions—DIZ and OA—which will be discussed in detail.

3.2.1 Direct Impinged Zone (DIZ)

The high-angle pure erosion damage occurring in the direct impinged zone (DIZ), was measured in terms of volume loss from the cathodically protected test samples. The low-alloy steel exhibited greater volume loss due to the high-angle pure erosion mechanism than the stainless steels—see

Table 3 H/E values and measured volume losses due to high-angle pure erosion for the tested materials

Material	H/E	H/K_{1C} ($m^{-1/2}$)	Volume loss due to high-angle pure erosion (mm^3)
UNS S31600	0.010	10	0.33
UNS S15500	0.018	44	0.34
UNS S32760	0.013	27	0.28
UNS G43400	0.015	39	0.50

Table 3. Similar trends have been observed in other studies [5, 24], where a medium carbon steel performed poorer than stainless steels under impingement erosion conditions. Marginal differences were observed when comparing the stainless steels, with the UNS S32760 exhibiting a slightly smaller volume loss than the UNS S15500 and the UNS S31600. The marginal differences between the stainless steels have been observed in terms of wear scar depths in a previous study [5]. By comparing the material's hardness in Table 2, no obvious linkage could be connected between the resistance to high-angle erosion and material hardness. A more widely accepted notion is the relationship between sliding abrasion resistance and hardness (H); this will be discussed later. Other theories suggest that the elastic modulus (E) and fracture toughness (K_{1c}) are material properties which are also important and that a high hardness to elastic modulus ratio or a high H/K_{1C} ratio are desirable [25–27]. However, in this study there was also no clear relationship between the H/E or H/K_{1C} ratios with the volume loss due to high-angle erosion (Table 3). The lack of correlation between conventional material properties and high-angle erosion resistance may be attributed to the high-strain rate conditions which occur during a high velocity impingement erosion-corrosion experiment [28].

From Figs. 8, 9, 10, it is evident that the dominant factor contributing to the volume losses in the DIZ was mechanical erosion. Indeed, the material loss of the low-alloy steel due to corrosion, erosion-enhanced corrosion and corrosion-enhanced erosion in the wear scar were found to be negligible at each salinity. In the DIZ, the contribution of the pure corrosion factor to overall material loss, calculated via Faraday's Law from the anodic polarisation scans of the segmented samples, as shown in Fig. 3 and in a previous study [16], was very small or negligible for all tested alloys at every salinity. Although, as displayed in Fig. 3, the passive films were being sporadically destroyed by impacting sand particles [29–31], it appears that the intermittent de-passivation/re-passivation events restricted the corrosion damage. The domination of erosion processes is likely to be associated with the size, shape and concentration of the sand as well as the velocity of the jet.

3.2.2 Outer Area (OA)

The pure sliding abrasion damage of the materials was calculated by subtracting the erosion damage in the DIZ under cathodic protection conditions from the total volume loss. The sliding abrasion damage has been illustrated in previous work [22]. Although there is often a link between high hardness and improved sliding abrasion resistance, the low-alloy steel, which exhibited the second greatest hardness, was found to have the poorest sliding abrasion resistance. This implies that the correlation between increased hardness and abrasion resistance is more complex than suggested in previous research [32–34]. Work conducted by Xu et al. [35] suggests that an increase in hardness of steels does not necessarily increase abrasion wear resistance and is in fact influenced more by grain size, grain morphology and amount of retained austenite.

3.2.2.1 Erosion-Enhanced Corrosion, ΔC_m For the UNS G43400 steel, there were some very distinct trends in this parameter that are attributable to the inherently poor corrosion resistance of this material that does not benefit from the establishment of a surface passive film. When the salinity was increased from 0.05%NaCl to 3.5%NaCl, there was a huge increase in ΔC_m in both hydrodynamic zones and this effect can be ascribed to the corrosion products being continuously swept off the surface by the impinging slurry which in turn exposes fresh, bare steel to the corrosive environment. Upon raising the salinity further to 10%NaCl, however, there was a small decrease in both the DIZ and the OA. These changes in ΔC_m with salinity mirror those in pure corrosion rates since the latter increased substantially from 0.05% to 3.5%NaCl but were unchanged upon the further increase in salinity to 10%NaCl (Figs. 8, 9, 10). These trends with salinity have been discussed elsewhere [16] in terms of less protective surface corrosion products at moderate salinities but the influence of competitive adsorption of Cl- ions and (OH)- at higher chloride concentrations.

For the stainless steels, trends in ΔC_m with salinity were much less clear cut and this is certainly associated with the extremely low/ negligible values for this parameter, due to the influence of the passive films. Even though these are being de-stabilised by the impacting sand particles, the re-passivation events are practically instantaneous, hence, this along with their higher alloying content, result in the extremely small/negligible erosion-enhanced corrosion.

3.2.2.2 Corrosion-Enhanced Abrasion, ΔM_C The low-alloy steel exhibited significant corrosion-enhanced abrasion damage in the OA at all salinities (17–21% of overall damage) but this proportion did not increase with salinity. This is likely to be associated with the observed corrosion rates remaining the same between 3.5%NaCl to 10%NaCl and this feature represents a similarity between the corrosion rate/ salinity trends between low-turbulence conditions [12–15] and impingement situations which have been discussed in detail elsewhere [16].

For the low-alloy steel, the corrosion-enhanced abrasion mechanisms can be attributed to the corrosion pits which are formed, as illustrated in a previous related study [22]. The pits cause local turbulence which enhances the mechanical erosion damage. Corrosion roughens the surface causing micro-turbulence, this would be exacerbated by corrosion pits [36].

Of the stainless steels, ΔM_C was negligible at the lowest salinity (hardly surprising given the also negligible pure corrosion rates) and was also low for the UNS S31600 grade at the higher NaCl concentrations. The UNS S15500 and UNS S32160 grades, however, exhibited significant increases in ΔM_C with increasing salinity attaining contributions to the overall material loss of 15–20%) at the highest salinity. These differences between the stainless steels can be attributed to the role of metallurgical structure in corrosion-enhanced erosion, as described below.

A reason for corrosion-enhanced abrasion in the austenitic stainless steel was suggested by Matsumura et al. [37] who suggested that corrosion removes the work hardened layer which in turn causes the stainless steel to be more susceptible to mechanical damage. Alternative explanations take account of the two-phase structure of two of the stainless steels. For example, the superduplex stainless steel is an example of a dual-phase material which can exhibit synergistic damage that is associated with micro-galvanic action at the phase boundaries. The latter phenomena has been shown in a number of erosion-corrosion systems, where the ferrite phase acts as an anode and the austenite phase acts as a cathode [38, 39]. Thus, an explanation for the involvement of such synergy in UNS S32760 and UNS S15500 is galvanic corrosion between the two or more different microstructural features (ferrite and austenite for UNS S32760 and martensite, retained austenite and precipitates for UNS S15500 steel) which allows easier removal of material from mechanical damage processes.

Table 4 Comparisons of volume losses recorded from single and segmented specimens of UNS G43400

% NaCl	Single specimen volume loss, mm^3	Segmented specimen, DIZ volume loss, mm^3	Segmented specimen OA volume loss, mm^3
0.05	1.30	0.45	0.85
3.5	3.42	0.49	2.93
10.0	2.95	0.53	2.42

3.3 Comparisons between Indications of Damage Contributions from Single and Segmented Specimens

As pointed out earlier, one of the potential limitations associated with submerged jet experiments, conducted on specimens/components in which the area of the directly impinged zone is less than the overall area, is that the findings essentially represent an "average" of effects experienced in distinctly different hydrodynamic regions.

Thus, for the low-alloy steel, the data in Figs. 5, 6, 7 demonstrate that the total volume loss increases from 0.05% to 3.5% NaCl but then displays a decrease at 10% NaCl. As shown in Table 4, however, this trend is only replicated in the volume losses recorded in the outer region of a segmented specimen and does not correlate with the values observed in the directly impinged zone. These effects are clearly associated with the different mechanisms of damage during erosion-corrosion. Thus, in the DIZ, at all salinities studied, the damage mechanism is almost entirely pure erosion. In contrast, the indications from a single specimen and from the OA measurements on a segmented specimen both reveal substantial contributions (over 60%) from corrosion-related ($C + \Delta C_m + \Delta M_c$) processes. In other words, the predictive behaviour obtained from a single specimen is more reliable indicator of damage in the OA but not so in the DIZ.

With regard to stainless steels, as Table 5 shows, all variants of damage assessment (single specimen, DIZ and OA) indicate a continuous increase in volume loss with % NaCl for each type of stainless steel. In terms of comparisons between the different alloys at any specific NaCl concentration, the single specimen data indicates slight increases in volume losses for the UNS S15000 compared to the austenitic UNS S31600 alloy but the material loss exhibited by the superduplex stainless steel was less than the other alloys. These trends are more in line with the material losses exhibited in the outer zones than for the DIZ where there was no distinct evidence of increased

Table 5 Comparisons of volume losses recorded from single and segmented specimens of the stainless steels

% NaCl	Single specimen volume loss, mm^3			Segmented specimen, DIZ volume loss, mm^3			Segmented specimen OA volume loss, mm^3		
	UNS S31600	UNS S15500	UNS S32760	UNS S31600	UNS S15500	UNS S32760	UNS S31600	UNS S15500	UNS S32760
0.05	0.70	0.75	0.60	0.33	0.34	0.28	0.35	0.38	0.35
3.5	0.75	0.80	0.65	0.39	0.37	0.31	0.37	0.45	0.40
10.0	0.90	1.0	0.75	0.48	0.41	0.34	0.46	0.61	0.45

material losses experienced by the UNS S15500 alloy compared to the UNS S31600 grade.

In summary, it appears that the use of a single specimen to obtain damage trends in most submerged jet experiments is likely to yield imprecise findings in some circumstances–especially in relation to the attack on the directly impinged zone. This feature has been noted in previous investigations [21–23, 40]. It is worthwhile noting that there is reasonable correlation between the material loss of single samples and the outer area. Such imprecision, in the prediction of damage in the directly impinged zone provided by data from single specimens, is particularly problematical when it is recognised that this is the region where the erosion-corrosion damage is at its most severe.

4 Conclusions

The work has provided some indications that the vulnerability of materials to corrosive wear may not be seriously increased in higher salinity (above 3.5%NaCl) aqueous solutions.

- The effect of increasing the salt content of an impinging slurry can be fairly complex both in terms of the influence on overall material loss but also in respect of varying effects on different materials and in different hydrodynamic zones of an impacted component.
- For the stainless steels, the majority of the damage was observed to be mechanical in both wear regions. This feature is obviously related to the relatively high corrosion resistance of these alloys. Nevertheless, there was a general increase in corrosion-related damage mechanisms with increased salinity. This was a result of the periodic de-passivation/re-passivation events which, in turn, was the basis of a significant proportion (up to 33% at 10%NaCl) of corrosion-enhanced material loss in the outer area.
- For the low-alloy steel, as the salt content was raised from 0.05%NaCl to 3.5%NaCl, the contribution of corrosion-related mechanisms to the overall damage was increased significantly. However, when the salinity was increased further to 10%NaCl, the overall damage was not intensified and in fact decreased. This influence of salinity was found, as expected, to be linked to corrosion-related damage. The influence of flow on increasing the corrosion rate, ΔCm, is obviously crucial but the role of corrosion in accelerating the mechanical damage also represents a less-obvious element of damage in low-angle corrosion abrasion situations.
- Additional "sensitivity" is obtained by the use of segmented specimens in avoiding somewhat oversimplified conclusions that may arise in some circumstances from the use of a single specimen. For instance, the findings using a single specimen were generally in accord with the behaviour in the outermost regions but with little, or no correlation to the damage experienced in the directly–impinged part of the component.

Acknowledgements The authors would like to acknowledge the support for this study, which was provided by the Weir Group PLC (WARC2011- SAA1, 2011) via its establishment of the Weir Advanced Research Centre (WARC) at the University of Strathclyde.

Declarations

Conflict of interest Authors declare no conflict of interest.

References

1. Zakowski K, Narozny M, Szocinski M, Darowicki K (2014) Influence of water salinity on corrosion risk - the case of the southern Baltic Sea coast. Environ Monit Assess 186:4871–4879. https://doi.org/10.1007/s10661-014-3744-3
2. Rassenfoss S (2011) From Flowback to Fracturing: Water Recycling Grows in the Marcellus Shale. J Pet Technol 63(7):48–51. https://doi.org/10.2118/0711-0048-JPT
3. Haibin L, Zhenling L (2010) Recycling utilization patterns of coal mining waste in China. Resour Conserv Recycl 54:1331–1340. https://doi.org/10.1016/j.resconrec.2010.05.005
4. Estrada JM, Bhamidimarri R (2016) A review of the issues and treatment options for wastewater from shale gas extraction by hydraulic fracturing. Fuel 182:292–303. https://doi.org/10.1016/j.fuel.2016.05.051
5. Giourntas L, Hodgkiess T, Galloway AM (2015) Comparative study of erosion–corrosion performance on a range of stainless steels. Wear 332–333:1051–1058. https://doi.org/10.1016/j.wear.2014.12.052
6. Aribo S, Barker R, Hu X, Neville A (2013) Erosion–corrosion behaviour of lean duplex stainless steels in 3.5% NaCl solution. Wear 302(1–2):1602–1608. https://doi.org/10.1016/j.wear.2012.12.007
7. Neville A, Hodgkiess T (1997) Study of effect of liquid corrosivity in liquid-solid impingement on cast iron and austenitic stainless steel. Br Corrosion J 32(3):197–205. https://doi.org/10.1179/000705997798114904
8. Neville A, Hodgkiess T, Xu H (1999) An electrochemical and microstructural assessment of erosion-corrosion of cast iron. Wear 233–235:523–534. https://doi.org/10.1016/S0043-1648(99)00225-2

9. Chen J, Wang J, Chen B, Yan F (2011) Tribocorrosion behaviors of Inconel 625 alloy sliding against 316 steel in seawater. Tribol Trans 54(4):514–522. https://doi.org/10.1080/10402004.2011.571362
10. Gou W, Zhang H, Li H, Liu F, Lian J (2018) Effects of silica sand on synergistic erosion caused by cavitation, abrasion, and corrosion. Wear 412–413:120–126. https://doi.org/10.1016/j.wear.2018.07.023
11. Revie RW, Uhlig HH (2008) Corrosion and Corrosion Control: An Introduction to Corrosion Science and Engineering, 4th edn. Hoboken, New Jersey
12. Cheng P, Huang X (2017) Effect of Salinity on Corrosion Behavior of DH36 Steel in Seawater Immersion Zone. DEStech Transactions on Engineering and Technology Research. https://doi.org/10.12783/dtetr/apetc2017/11221
13. Uhlig HH, Morrill MC (1941) Corrosion of 18–8 Stainless Steel in Sodium Chloride Solutions. Ind Eng Chem 33(7):875–880. https://doi.org/10.1021/ie50379a013
14. Sani F. M., Brown B., Belarbi Z., and Nesic S. (2019) An experimental investigation on the effect of salt concentration on uniform CO2 corrosion. NACE International Corrosion Expo. 2019 Paper 13026.
15. Fang H., Brown B., and Nesic S. (2010) High salt concentration effects on CO2 corrosion and H2S Corrosion. NACE International Corrosion Expo. 2010 Paper 10276.
16. Brownlie F., Hodgkiess T., Pearson A., Galloway A. M. (2021) Electrochemical evaluation of the effect of different NaCl concentrations on low alloy- and stainless steels under erosion-corrosion conditions. Corrosion–under review.
17. ASTM G119–09 (2009) Standard for determining synergism between wear and corrosion. ASTM International, West Conshohocken, PA
18. Aminul Islam Md, Farhat ZN, Ahmed EM, Alfantazi AM (2013) Erosion enhanced corrosion and corrosion enhanced erosion of API X-70 pipeline steel. Wear 302:1592–1601. https://doi.org/10.1016/j.wear.2013.01.041
19. Guo HX, Lu BT, Luo JL (2005) Interaction of mechanical and electrochemical factors in erosion-corrosion of carbon steel. Electrochemica Acta 51:315–323. https://doi.org/10.1016/j.electacta.2005.04.032
20. Aminul Islam Md, Farhat ZN (2013) The synergisitic effect between erosion and corrosion of API pipeline in CO_2 and saline medium. Tribol Int 68:26–34. https://doi.org/10.1016/j.triboint.2012.10.026
21. Giourntas L, Hodgkiess T, Galloway AM (2015) Enhanced approach of assessing the corrosive wear of engineering materials under impingement. Wear 338–339:155–163. https://doi.org/10.1016/j.wear.2015.06.004
22. Smith F, Brownlie F, Hodgkiess T, Toumpis A, Pearson A, Galloway AM (2020) Effect of salinity on the corrosive wear behaviour of engineering steels in aqueous solutions. Wear. https://doi.org/10.1016/j.wear.2020.203515
23. Brownlie F, Anene C, Hodgkiess T, Pearson A, Galloway AM (2018) Comparison of Hot Wire TIG Stellite 6 weld cladding and lost wax cast Stellite 6 under corrosive wear conditions. Wear 404–405:71–81. https://doi.org/10.1016/j.wear.2018.03.004
24. Neville A, Hodgkiess T, Dallas JT (1995) A study of the erosion-corrosion behaviour of engineering steels for marine pumping applications. Wear 186–187:497–507. https://doi.org/10.1016/0043-1648(95)07145-8
25. Ben-Ami Y, Uzi A, Levy A (2016) Modelling the particles impingement angle to produce maximum erosion. Powder Technol 301:1032–1043. https://doi.org/10.1016/j.powtec.2016.07.041
26. Chintha AR, Valtonen K, Kuokkala VT, Kundu S, Peet MJ, Bhadeshia HKDH (2019) Role of fracture toughness in impact abrasion wear. Wear 428–429:430–437. https://doi.org/10.1016/j.wear.2019.03.028
27. Leyland A, Matthews A (2000) On the significance of the H/E ratio in wear control: a nanocomposite coating approach to optimised tribological behaviour. Wear 246(1–2):1–11. https://doi.org/10.1016/S0043-1648(00)00488-9
28. Sundararajan G (1995) The solid particle erosion of metallic materials: The rationalization of the influence of material variables. Wear 186–187:129–144. https://doi.org/10.1016/0043-1648(95)07172-5
29. Zheng ZB, Zheng YG (2016) Erosion-enhanced corrosion of stainless steel and carbon steel measured electrochemically under liquid and slurry impingement. Corros Sci 102:259–268. https://doi.org/10.1016/j.corsci.2015.10.014
30. Hu X, Neville A (2005) The electrochemical response of stainless steels in liquid-solid impingement. Wear 258:641–648. https://doi.org/10.1016/j.wear.2004.09.043
31. Rajahram SS, Harvey TJ, Wood RJK (2011) Electrochemical investigation of erosion-corrosion using a slurry pot erosion tester. Trib Int 44:232–240. https://doi.org/10.1016/j.triboint.2010.10.008
32. Stevenson ANJ, Hutchings IM (1995) Wear of Hardfacing While Cast Irons By Solid Particle Erosion. Wear 186(1):150–158. https://doi.org/10.1016/0043-1648(95)07184-9
33. Llewellyn RJ, Yick SK, Dolman KF (2004) Scouring erosion resistance of metallic materials used in slurry pump service. Wear 256(6):592–599. https://doi.org/10.1016/j.wear.2003.10.002
34. Giourntas L., Brownlie F., Karafyllias G., Hodgkiess T., and Galloway A. M. (2016) Effect of corrosion on abrasive wear in a range of materials. BHR Group–23rd International Conference on Fluid Sealing 2016.
35. Xu X, Xu W, Ederveen FH, Van Der Zwaag S (2013) Design of low hardness abrasion resistant steels. Wear 301(1–2):89–93. https://doi.org/10.1016/j.wear.2013.01.002
36. Harvey TJ, Wharton JA, Wood RJK (2007) Development of synergy model for erosion–corrosion of carbon steel in a slurry pot. Tribology 1(1):33–47. https://doi.org/10.1179/175158407X181471
37. Matsumura M (2012) Erosion-Corrosion: An Introduction to Flow Induced Macro-Cell Corrosion. Bentham Science Publishers. https://doi.org/10.2174/97816080535131120101
38. Lee J-S, Fushimi K, Nakanishi T, Hasegawa Y, Park Y-S (2014) Corrosion behaviour of ferrite and austenite phases on super duplex stainless steel in a modified green-death solution. Corros Sci 89:111–117. https://doi.org/10.1016/j.corsci.2014.08.014
39. Yau YH, Streicher MA (1987) Galvanic corrosion of duplex FeCr-10%Ni alloys in reducing acids. Corrosion 43(6):366–373. https://doi.org/10.5006/1.3583872
40. Brownlie F, Hodgkiess T, Pearson A, Galloway AM (2017) Effect of nitriding on the corrosive wear performance of a single and double layer Stellite 6 weld cladding. Wear 376–377:1279–1285. https://doi.org/10.1016/j.wear.2017.01.006